A Pharmacophore Model for SARS-CoV-2 3CLpro Small Molecule Inhibitors and in Vitro Experimental Validation of Computationally Screened Inhibitors

Enrico Glaab*[†1], Ganesh Babu Manoharan[2], Daniel Abankwa[*2]

[1]Luxembourg Centre for Systems Biomedicine (LCSB), University of Luxembourg, 7 avenue des Hauts Fourneaux, L-4362 Esch-sur-Alzette, Luxembourg

[2]Department of Life Sciences and Medicine, University of Luxembourg, 7 avenue des Hauts Fourneaux, L-4362 Esch-sur-Alzette, Luxembourg

[*]EG and DA are joint senior authors

[†]Contact: enrico.glaab@uni.lu

Abstract

Among the biomedical efforts in response to the current coronavirus (COVID-19) pandemic, pharmacological strategies to reduce viral load in patients with severe forms of the disease are being studied intensively. One of the main drug target proteins proposed so far is the SARS-CoV-2 viral protease 3CLpro (also called Mpro), an essential component for viral replication. Ongoing ligand- and receptor-based computational screening efforts would be facilitated by an improved understanding of the electrostatic, hydrophobic and steric features that characterize small molecule inhibitors binding stably to 3CLpro, as well as by an extended collection of known binders.

Here, we present combined virtual screening, molecular dynamics simulation, machine learning and in vitro experimental validation analyses which have led to the identification of small molecule inhibitors of 3CLpro with micromolar activity, and to a pharmacophore model that describes functional chemical groups associated with the molecular recognition of ligands by the 3CLpro binding pocket. Experimentally validated inhibitors using a ligand activity assay include natural compounds with available prior knowledge on safety and bioavailability

1

properties, such as the natural compound rottlerin (IC_{50} = 37 μM), and synthetic compounds previously not characterized (e.g. compound CID 46897844, IC_{50} = 31 μM). In combination with the developed pharmacophore model, these and other confirmed 3CLpro inhibitors may provide a basis for further similarity-based screening in independent compound databases and structural design optimization efforts, to identify 3CLpro ligands with improved potency and selectivity.

Overall, this study suggests that the integration of virtual screening, molecular dynamics simulations and machine learning can facilitate 3CLpro-targeted small molecule screening investigations. Different receptor-, ligand- and machine learning-based screening strategies provided complementary information, helping to increase the number and diversity of identified active compounds. Finally, the resulting pharmacophore model and experimentally validated small molecule inhibitors for 3CLpro provide resources to support follow-up computational screening efforts for this drug target.

Keywords

COVID-19, SARS-CoV-2, pharmacophore, drug repurposing, 3CLpro, ligand activity assay, virtual screening, molecular dynamics simulation, machine learning

INTRODUCTION

The coronavirus disease 2019 (COVID-19), caused by the severe acute respiratory syndrome coronavirus 2 (SARS-CoV-2), represents a major challenge for health care systems around the world. Patients experience highly heterogeneous symptoms, ranging from asymptomatic forms and mild symptoms of a respiratory infection to severe illness, which can lead to hospitalization and death.

While the first vaccines against COVID-19 have received Emergency Use Authorization (EUA) by the Food and Drug Administration (FDA) and mass vaccination campaigns are currently ongoing, the available drug-based treatments for the disease are still limited. In the RECOVERY trial, a randomized trial designed to provide a fast and robust assessment of potential treatments for COVID-19, the corticosteroid dexamethasone was associated with a reduced mortality for patients with severe forms of the disease, when using a moderate dose (6 mg daily for 10 days) [1]. The FDA has included dexamethasone in their list of drugs used for hospitalized patients with COVID-19, and the European Medicines Agency (EMA) has endorsed the use of dexamethasone in patients from twelve years of age and weighing at least 40 kg, who require supplemental oxygen therapy. Moreover, the drug remdesivir, which inhibits the viral RNA-dependent RNA-polymerase (RdRp), was approved by the FDA for the treatment of COVID-19 requiring hospitalization. Remdesivir provided a statistically significant shorter median time to recovery in the clinical trial ACTT-1 [2], and significant symptom improvements vs. the standard of care in the GS-US-540-5774 trial [3], but no statistically significant improvements were observed for overall 29-day mortality in the ACTT-1 trial. In the independent SOLIDARITY trial no significant benefits were found in terms of reduced mortality, reduced initiation of ventilation or hospitalization

3

duration [4]. Other potential treatment options against COVID-19 studied in clinical trials, such as tocilizumab [5], colchicine [6], synthetic neutralizing antibodies [7], or convalescent plasma [8], among others, were at the time of writing still under investigation. Overall, while first significant successes in COVID-19 treatment have been achieved using pharmacological methods, there is a broad consensus that additional primary or adjuvant treatment approaches are required to further reduce mortality and hospitalization rates.

For the development of new drug therapies against COVID-19 both human and viral protein drug targets have been proposed. Suggested human drug targets include in particular proteins involved in mediating the entry of SARS-CoV-2 into the cell, such as the proteases TMPRSS2 and FURIN, which have been implicated in the proteolytic processing of the viral spike protein before cell entry [9,10]. The viral targets mainly include proteins involved viral replication (3CLpro / Nsp5 [11], PLpro / Nsp3 [12], RdRp / Nsp12 [13], Hel / Nsp13 [14]), and proteins associated with viral cell entry (S1, S2 [15]) and release (ORF3a [16,17]).

One of the viral targets of particular interest is the 3C-like protease (3CLPro, Mpro), which is needed by SARS-CoV-2 for the cleavage of viral polyproteins into 11 non-structural proteins (NSPs) that are essential for viral replication [11]. Apart from its critical role in replication, 3CLPro may also represent a well-suited target for drug development, because multiple crystal structures are available with high resolution (< 1.3 Å) and favorable quality characteristics, and first small molecule inhibitors for both the SARS-CoV-2 and SARS-CoV forms of the protein have already been identified [18–21]. While these inhibitors still have limitations in terms of either their binding affinity for the target protein, their bioavailability, adverse drug effects or high manufacturing

4

costs, the existing structural data for 3CLPro provides ample opportunities to apply both receptor- and ligand-based computational screening approaches in order to identify more potent and selective inhibitors.

To contribute to the ongoing research efforts on identifying improved 3CLPro inhibitors, here we present the results of a combined computational and experimental screening and pharmacophore generation approach. By integrating multiple computational approaches for molecular docking, ligand-based screening, machine learning and Molecular Dynamics (MD) simulations, we have ranked small molecule compounds from the public libraries provided by the repositories ZINC [22], SWEETLEAD [23] and the company MolPort (www.molport.com) as candidate inhibitors for 3CLPro. Top-ranked compounds and a few reference molecules previously proposed as 3CLpro inhibitors in the literature were experimentally assessed using a ligand activity assay to identify a subset of inhibitors and their IC_{50} values. We also compared the utility of different strategies for inhibitor discovery on the MolPort library. This extended analysis focused only on the MolPort compounds, because this library was our main resource for commercially available compounds and therefore of particular relevance for the experimental studies, and due to its smaller size (~7.7 million compounds), an extension to more computationally demanding screening approaches was still feasible in terms of runtime requirements. Finally, the validated inhibitors, which include both natural compounds with existing information on ADMETox characteristics, as well as previously uncharacterized synthetic compounds, were used to generate a pharmacophore model (i.e. a computational model that describes the steric and chemical features of compounds associated with the binding to the target protein).

The information derived from this model and the confirmed inhibitors provide a resource to facilitate follow-up efforts on the structural design of more potent and selective 3CLpro inhibitors or the similarity-based inhibitor screening in additional compound databases.

The reader should note that the workflows used for computational screening in the present study are limited by their design for typical high-performance computing systems in an academic setting. Recent supercomputer-based virtual screening approaches, which have also been applied to 3CLpro inhibitor screening, can explore a significantly wider search space of compounds and conformations, and therefore also have the potential to achieve higher hit rates. Specifically, supercomputing-based screening methods have recently been shown to enable an improved modeling of 3CLpro receptor flexibility using ensemble docking [24], extensive MD simulations to generate high-resolution conformational ensembles [25], and the application of more advanced polarizable force fields [26]. Similarly, for the experimental assessment of 3CLpro inhibitory activity, recently developed assays published during the writing time of this manuscript provide a higher scalability and throughput than the Förster resonance energy transfer (FRET) assay used in the present work, and have already identified new 3CLpro inhibitors as drug candidates for further development [20].

Because supercomputing facilities and more recent inhibition assays were not available to us, the goal of our study was to contribute to research on inhibiting SARS-CoV-2 3CLpro by providing complementary results and data with the methods and hit rates achievable in an academic setting, in particular through the computational discovery and experimental confirmation of new micromolar 3CLpro inhibitors, and through the creation of pharmacophore models specific to the conformational and

physicochemical properties of these inhibitors. The identified inhibitors and the information from the pharmacophore model provide both an input to support further screening studies, e.g. using independent private compound libraries, and a basis for the rational design of compounds with improved activity and ADMETox properties. The potential for further structural optimization of initial screening hits has recently already been illustrated in a study using computational lead optimization of the weak hit compound perampanel for 3CLpro inhibition, which led to the design and confirmation of multiple noncovalent, nonpeptidic 3CLpro inhibitors with significantly improved affinity in a kinetic assay, that were successfully confirmed to inhibit infectious SARS-CoV-2 replication *in vitro* [21,27].

In the following sections, we first present the computational and experimental methods used for screening and compound validation, the results of the screening procedure in terms of the characteristics of the validated inhibitors, and finally a discussion of the pharmacophore model generated from the analysis of these confirmed inhibitors.
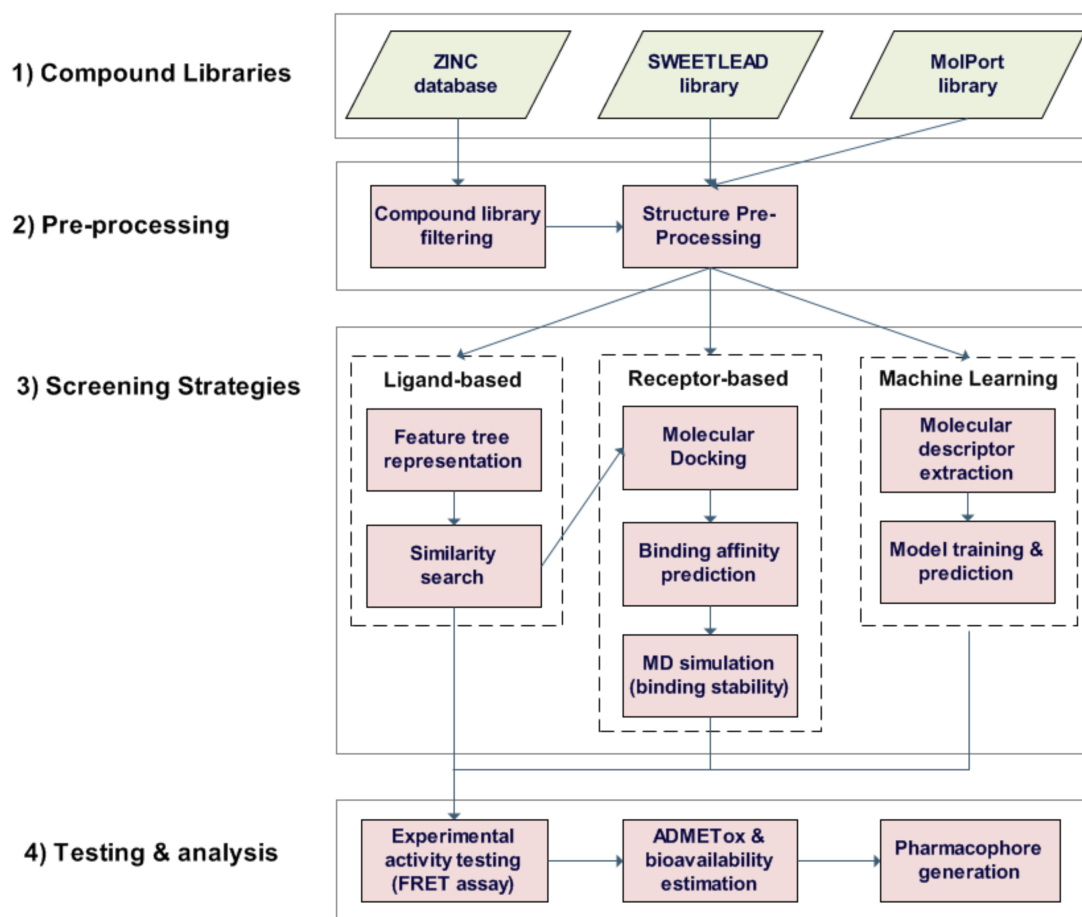
METHODS

In order to identify and characterize small molecule inhibitors for SARS-CoV-2 3CLpro and build a pharmacophore model, a multi-step computational screening procedure was combined with subsequent ligand activity assay experiments. The main component of the computational screening consisted of a filtering procedure involving multiple receptor- and ligand-screening approaches in combination with a final molecular dynamics (MD) simulation to confirm the stability of the binding for the top-

ranked compounds and docking poses. An overview of this part of the screening approach is shown in Figure 1, the detailed methodology, including the prior preprocessing of protein and compound structures, is discussed in the following sections below. Additionally, as part of the *in silico* selection of candidate compounds for experimental validation, the structural bioinformatics based screening was complemented by a machine learning approach for compound selection, using a training set of molecular descriptor data derived from known binders and non-binders for 3CLPro. This complementary screening approach is presented in detail in the section 'Machine learning based compound screening' below.

The compounds prioritized using these *in silico* screening methods were then evaluated experimentally to determine the subset of stable binders and their 3CLpro inhibitory activity, using an *in vitro* Förster-type resonance energy transfer (FRET) assay. These experimental analyses are described in more detail in the section '*in vitro* assay for 3CLpro inhibitory activity assessment'.

Figure 1. Overview of overall workflow for the screening procedure, starting with a compound library of > 1 billion compounds from the databases ZINC, SWEETLEAD and the MolPort. Due to the large size of the ZINC database, this compound repository was pre-filtered to focus on compounds that are commercially available and have drug-like chemical and ADMETox properties, and receptor-based screening was only applied after prior ligand-based screening (see section on 'Ligand pre-processing and filtering'). More computationally expensive approaches relying only on receptor-based screening were only applied to the smaller SWEETLEAD and MolPort libraries, and machine learning based compound screening was only applied to the MolPort library (see sections on 'Receptor-based screening using molecular docking' and 'Machine learning based compound screening'). A final selection of 95 top-ranked compounds derived from the *in silico* screening approaches was tested experimentally using a FRET assay to assess the 3CLpro inhibitory activity. Confirmed active compounds were characterized in terms of their known or computationally estimated ADMETox and bioavailability properties. Finally, pharmacophore models were generated for the active compounds.

COMPUTATIONAL METHODS

Protein structure pre-processing

Three publicly available protein crystal structures for 3CLPro from the Protein Data Bank [28] were chosen for the molecular docking analyses and binding affinity estimation (PDB: 5R8T, 6YB7 and 6LU7). The structures 5R8T and 6YB7 were selected mainly due to their resolution (5R8T: 1.27 Å, 6YB7: 1.25 Å) and quality (R-free value: 0.208 for 5R8T and 0.192 for 6YB7), see additional quality assessments described below), whereas the structure 6LU7 was used additionally as a representation of the holo form of the protein in complex with an inhibitor (resolution: 2.16 Å, R-free value: 0.235), allowing us to compare docking results across different types of structures. Since many previously reported 3CLpro inhibitors are allosteric inhibitors [29–31], and allosteric inhibitors have been proposed to disrupt the 3CLpro dimer or slow the rate of processing significantly [29], we did not focus specifically on targeting the 3CLpro dimerization interface, but aimed to cover all binding pockets associated with already identified small molecule inhibitors. As an alternative approach, for the SARS-CoV version of 3CLpro, previous studies have also investigated peptide inhibitors designed specifically to target the dimerization [32,33].

The receptor structures were pre-processed using the Schrödinger Maestro software (version 11.8.0.1.2, www.schrodinger.com) by adding hydrogens, generating protonation states, and optimizing hydrogen positions using the 'Protein Preparation Wizard' with default settings. The quality of the original and processed structures was assessed using the software tools Verify3D [34], WHATCHECK [35] and PROCHECK [36] as implemented in the software SAVES 5.0 (http://servicesn.mbi.ucla.edu/SAVES), confirming the suitability of the structures for docking simulations in terms of common

10

quality control checks [37]. For structure files containing multiple chains, the chain with the highest Verify3D score was chosen for further analysis.

Ligand pre-processing and filtering

Small molecule compounds were obtained from the databases ZINC (version: ZINC15, May 2020, [22]), SWEETLEAD (version: 1.0, [23]), and the public library provided by the company MolPort (May 2020, www.molport.com). All ligands from the SWEETLEAD database were first preprocessed using the AutoDock ligand preparation script, and docked into the 3CLpro binding pocket using AutoDock-GPU [38]. For the ZINC database, in order to focus on compounds that are commercially available and have drug-like chemical and ADMETox properties, a filtering was first applied by downloading only compounds with the properties "drug-like", "purchasable" (minimum purchasability = "Wait OK") and reactivity = "clean". This first-step filtering reduced the initial 1,276,766,435 substances to 898,838,573 retained substances. These filtered compounds were downloaded in SMILES-format, using the "ZINC-downloader-2D-smi.wget" script derived from the "Tranches" web-page on ZINC (https://zinc.docking.org/tranches/home).

The pre-selection of compounds from ZINC was then further filtered using a ligand-based similarity screening. For this purpose, a similarity assessment approach involving a graph-based molecular representation known as "feature trees" was applied, as implemented in the BioSolveIT Ftrees software (version 6.2). With this method the topological and physicochemical similarity of the library compounds to known small-molecule inhibitors for 3CLpro reported in the literature was scored (considering inhibitors for both the SARS-CoV and SARS-CoV-2 versions of the 3CLpro

protein). Specifically, the literature-derived query compounds include the reported *SARS-CoV-2* 3CLpro inhibitors GC-376 [18], ebselen [39,40] and baicalein [41], and the reported *SARS-CoV* 3CLpro inhibitors amentoflavone [42], hesperetine [43], pectolinarin [44] and dieckol [45]. Moreover, to further extend the search space of potential candidate inhibitor compounds, four additional query compounds for the feature tree search were included by adding the top-ranked compounds from the initial AutoDock-GPU screening (see above). All compounds from the ZINC library exceeding a minimum similarity threshold of 0.8 in the FTrees screen to these query compounds were retained for the subsequent molecular docking analyses.

For the screening of the MolPort compound library, due its association with our main provider for the commercial ordering of compounds and its smaller size (~7.7 million compounds) compared to the ZINC library, we tested multiple alternative more extensive screening approaches without prior library filtering: (1) a screening approach relying purely on fast molecular docking approaches (see details in following section), (2) a screening approach relying purely on machine learning (see section on 'Machine learning based compound screening' below), and (3) a combination of molecular docking and ligand-similarity based screening using the software FTrees (following the same approach as for the ZINC database, but without prior database filtering, and focusing on the most potent available 3CLPro inhibitor, GC-376, as query compound; see following section for the description of the docking analyses).

Conformers for the collected compounds were generated using the OpenEye OMEGA software (version: 3.1.2.2, http://www.openeye.com) using the classic mode with default parameters.

Receptor-based screening using molecular docking

In order to obtain a robust ranking of compounds using molecular docking, the compound libraries prepared in the previous step (i.e. the filtered version of the ZINC database, and the unfiltered SWEETLEAD and MolPort databases) were docked into the 3CLpro binding pocket using three different approaches, AutoDock-GPU (an OpenCL and Cuda accelerated version of AutoDock4.2.6, [38]), OpenEye HYBRID (version 3.4.0.2, [46–48]), and LeadIT/FlexX (version 2019.Nov.2-Ubuntu-18.04-x64, [49]). To use the available computing time efficiently and only consider compounds with high relative ranking scores for all docking approaches for further analysis, the two most time-efficient docking methods AutoDock-GPU (with the parameter 'nrun' for the thoroughness of the search space exploration set to 100, and default parameters otherwise) and OpenEye HYBRID (with default docking parameters) were first run on the pre-selected compound libraries, and only compounds with higher than average scores from the AutoDock-GPU and OpenEye HYBRID screens were also docked using FlexX (with default docking parameters), including a subsequent estimation of the binding affinity for the top 30 docking poses using the LeadIT/HYDE approach [50]. The docking methods are semi-flexible, taking ligand flexibility into account; however, as a limitation in contrast to recent supercomputer-based screening approaches, which address receptor flexibility using high-resolution ensembles of many 3CLpro receptor conformations [25], ensemble docking and enhanced sampling MD [24], the assessment of receptor flexibility in the present study was restricted to the MD simulations applied to the top-ranked compounds derived from the docking analyses (see section on 'Molecular dynamics simulations').

For the MolPort library, we compared both a screening approach relying purely on molecular docking of the unfiltered library, and a joint docking and ligand similarity-based scoring approach, which filtered the compounds by including only those reaching a minimum similarity threshold of 0.8 in the ligand-based screening using FTrees (see previous section). Finally, the list of compounds docked with each method was ranked and sorted according to the sum of ranks across the scores for all methods. Only top-ranked compounds achieving consistently high docking scores for the three pre-processed 3CLpro protein structures (PDB: 5R8T, 6YB7 and 6LU7) were used for experimental validation. Visualizations of the top-scoring docked compounds were generated in the software Chimera (version 1.12, [51]) and binding interactions were analyzed using PoseView (version 1.1.2, [52]). A list of all used software tools and their versions, as well as scripts including the commands and parameters for the virtual screening analyses are provided on GitHub (https://github.com/eglaab/3clpro).

Molecular dynamics simulations

To assess the ligand binding stability for the top-ranked compounds derived from the docking simulations in the 3CLpro binding pocket, molecular dynamics (MD) simulations were carried out using a GPU-accelerated version of the software NAMD (Git-2020-07-30 for Linux-x86_64-multicore-CUDA, [53]). Topology and force field parameters for the MD simulations were assigned from the CHARMM36 protein lipid parameter set [54,55] for the receptor and from the CHARMM General Force Field (CGenFF) parameter set [56] for the ligands. The step size was 2 fs, and the simulation was performed for a duration of 20 ns. Video animations of the simulations were created by applying the "MD Movie" function in the software Chimera (version 1.12,

build 41623, [51]) to the trajectory data for the protein-ligand complexes derived from NAMD. The detailed configuration settings used for NAMD and exemplary video animations of MD simulations for confirmed inhibitors are provided on GitHub (https://github.com/eglaab/3clpro).

Machine learning based compound screening

As an alternative to conventional receptor- and ligand-based screening strategies, we also tested a compound ranking approach using machine learning. For this purpose, quantitative properties for the investigated compounds were determined by calculating molecular descriptors as implemented in the R software package "rcdk" (version 3.5.0) [57] using SMILES compound representations [58] as input. First, molecular descriptors were computed for a previously published training set collection of small molecules containing both previously reported SARS-CoV or SARS-CoV-2 3CLPro inhibitors (486 compounds, used as positive set) and compounds reported not to bind to 3CLPro (700 compounds, used as negative set) [59]. The covered classes of descriptors in the package "rcdk" include topological descriptors (e.g. TPSA, Wiener index, Kier-Hall Smarts descriptor), geometrical (e.g. gravitational index, Petitjean shape index, moment of inertia), electronic (e.g. CPSA, H-bond donor count, H-bond acceptor count), constitutional (e.g. rotatable bond count, acidic group count, weight) and hybrid descriptors (WHIM and BCUT descriptors; see the documentation of the rcdk software package to retrieve the complete list of more than 200 descriptors).

A classification model using the Random Forest algorithm as implemented in the R software package "randomForest" (version 4.6-14, [60]) was then built on this training

data of molecular descriptors for the positive and negative compound sets, using 250 decision trees and default settings otherwise. This model was applied to all compounds from the MolPort library, by computing the descriptors for each compound as input to the model and generating probabilistic predictions. Finally, the predicted probability for each compound to belong to the positive set of 3CLPro inhibitors was used to rank the compounds, and the top 20 compounds with the highest probabilities were selected for *in vitro* testing. A script for the machine learning analyses has been made available on GitHub (https://github.com/eglaab/3clpro).

EXPERIMENTAL METHODS

In vitro assay for assessing the 3CLpro inhibitory activity of the compounds

Assay principle: Förster resonance energy transfer (FRET) assays can be applied in various configurations in cells [61] and in reporter systems [62] to detect molecular proximity and with the proper biosensor also activity. Here we employed an *in vitro* FRET assay for the evaluation of the candidate small molecule inhibitors for 3CLpro obtained from the *in silico* screening approaches. We used a substrate peptide of 3CLpro labelled with a fluorescent dye (Dabcyl) and an acceptor-quencher (Edans) at the N- and C-terminus, respectively. The substrate peptide does not fluoresce in the uncleaved state, when the quencher blocks the fluorescence of the dye. When 3CLpro cleaves the substrate, the fluorescence of the dye is de-quenched and an emission signal is observed. The inhibitor blocking the activity of 3CLpro prevents FRET-peptide cleavage. Thus, in the presence of an inhibitor a lower fluorescence signal is observed [63]. A similar FRET-based assay has recently been applied to test candidate 3CLpro

16

inhibitor compounds derived from the lead optimization of a prior week screening hit, and some of these compounds were also successfully confirmed to inhibit infectious SARS-CoV-2 replication in Vero E6 cells [21,27]. Moreover, after the completion of our experimental studies, an optimized assay for high-throughput screening of 3CLpro using a new fluorogenic substrate became available [20]. This assay has been used to identify two irreversible 3CLpro inhibitors, azanitrile (K_i = 24.0 nM) and pyridyl ester (K_i = 10.0 nM) [20], as candidates for further development and provides a more scalable methodology than the one applied in the present study. Thus, for follow-up *in vitro* screening studies of 3CLpro inhibitors, more recently developed assays may be preferred over the assay with lower throughput employed here.

Method: The assays were performed following the guidelines of the 3CL Protease assay Kit (#79955, BPS Biosciences, San Diego CA, USA). The inhibitory effect on 3CLpro was assessed using the substrate peptide Dabcyl-KTSAVLQSGFRKM-E(Edans)-NH2, obtained from Biosyntan. The assays were run on a 384-well plate (black, low volume, round bottom; Corning #4514) and the reaction volume per well was 20 µl. Briefly, all candidate inhibitors were dissolved in DMSO and three-fold or five-fold diluted in the assay buffer. The known 3CLpro inhibitor and reference compound GC-376 was dissolved in water and diluted from 100 µM. To the dilution series of inhibitors, 3CLpro (100 ng/reaction) was added and incubated for 30 min at room temperature (RT). Then 50 µM of substrate peptide was added. The reaction mix was incubated at RT overnight with the plates sealed. On the next day, fluorescence intensity was measured at excitation wavelength 360 ± 10 nm and emission 460 ± 20 nm using Clariostar (BMG Labtech, Germany) plate reader. 3CLpro used in the assay

was N-terminally MBP-tagged (MW – 77.5 kDa) and obtained from BPS Biosciences (#100707). The data were fit into a log c(inhibitor) vs response three-parameter dose-response model using the software Prism (GraphPad). IC$_{50}$ value estimates were determined individually for each replicate, and the mean and standard error of the mean (SEM) were calculated. Importantly, many of the assessed compounds were polyaromatic natural products, which exhibited interfering fluorescence or absorbance in our FRET-based assay. Therefore, out of 96 compounds tested in the 3CLpro activity assay, 12 compounds were filtered out from further analysis (highlighted in blue color in the lists of tested compounds in the Supporting Information). Assays involving principles of time-resolved FRET may be suitable for future follow-up screening of compounds with background fluorescence [64,65].

RESULTS AND DISCUSSION

In silico screening results and final compound selection for in vitro testing

For the experimental testing of candidate 3CLPro small molecule inhibitors, 86 commercially available compounds selected from the top-scoring candidates derived from the different receptor-, ligand- and machine learning based screening approaches (see Methods), which had passed all prior *in silico* filtering stages, were ordered from the company MolPort. The complete list of tested screening compounds, including common compound identifiers and characteristics (SMILES, molecular weight, logP) is provided in the Supporting Information. The 86 top-ranked compounds are subdivided into 18 compounds derived from the virtual screening of the ZINC and SWEETLEAD libraries (Table S2 in the Supporting Information; see Methods for the prefiltering and screening approaches), 30 compounds derived from
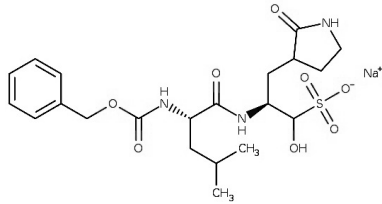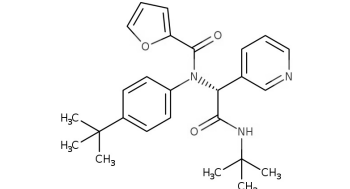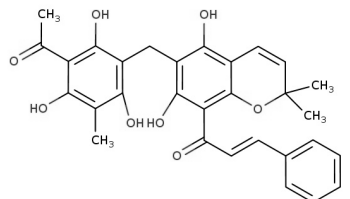
the screening of the MolPort library using combined ligand similarity screening and molecular docking (Table S3), 18 compounds from the screening of the MolPort library using combinations of docking algorithms only (Table S4), and 20 compounds from the purely machine learning derived compound ranking for the MolPort library (Table S5). In addition to these screening-derived compounds, the known inhibitor GC-376 [18] was included as a reference compound, and the following commercially available compounds previously reported as SARS-CoV-2 or SARS-CoV 3CLPro inhibitors in the literature, were also acquired for experimental inhibitory activity assessments: Ebselen [39,40], baicalein [41], amentoflavone [42], hesperetine [43], pectolinarin [44], luteolin [42], quercetin [42], pristimerin [66], and 1-hydroxypyridine-2-thione zinc [67]. For the compounds confirmed as binders (see Table 1), PAINS and Brenk's substructure alerts [68,69] were checked to determine frequent hitters (promiscuous compounds, see Table 2). GC-376 is a prodrug that converts into the peptide aldehyde GC-373 [70]; hence, the active compound is GC-373, and the inhibitor is therefore referred to as "GC-376 / GC-373" in the following. Example video animations of the MD simulations which were applied to the top-ranked docking-derived compounds to confirm the stability of the binding are provided online together with the configuration settings used for the MD simulation software NAMD (https://github.com/eglaab/3clpro).
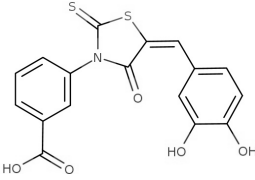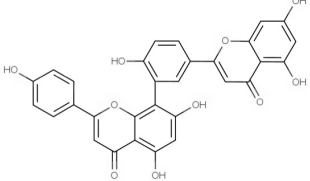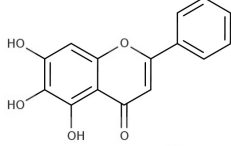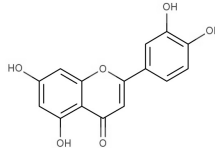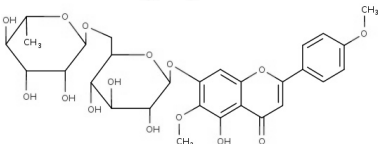
In vitro testing results for candidate 3CLpro inhibitors

In total, 95 selected compounds were assessed to determine their *in vitro* 3CLpro inhibitory activity, including the 86 candidate compounds identified from the *in silico* analyses and 9 candidate compounds derived from the literature, as described above.

GC-376 was used as a positive control for 3CLpro inhibitory activity. The IC_{50} value of GC-376 was in the low micromolar range (0.18 to 0.98 µM), matching approx. with previously reported IC_{50} values for GC-376 (0.19 µM) and its structurally similar metabolized form, GC-373 (0.4 µM) [70] (see Supporting Information for the dose-response curves). The Z' value [71], used as a measure of assay robustness, ranged from 0.5 to 0.8, indicating the suitability of the assay for compound screening in a high-throughput format. Importantly, the main purpose of the activity assay is to obtain a robust relative ranking of ligands in terms of their inhibitory activity rather than high precision absolute activity estimates.

Table 1: Hits from 3CLpro screening assay with IC_{50} values. *For the compounds no. 1 and 3 only a limited amount of the reagent could be acquired, and therefore no replicate runs could be performed for these specific compounds.

#	Compounds	Molport ID	IC_{50} (Mean ± SEM) / µM	Structure
	GC-376 (prodrug for GC-373)	MolPort-046-767-490	1.2 ± 0.3	
1	M-8524	MolPort-047-408-524	31*	
2	rottlerin	MolPort-003-959-457	37.0 ± 0.6	

20

3	M-1805	MolPort-000-821-805	100*	
4	amentoflavone	MolPort-001-741-078	143 ± 23	
5	baicalein	MolPort-001-741-408	208 ± 55	
6	luteolin	MolPort-000-706-683	343 ± 77	
7	pectolinarin	MolPort-007-980-807	468 ± 58	

Overall, 7 out of the 95 tested compounds were confirmed as active, with a lowest IC$_{50}$ of 31 μM for the screening compound M-8524 (CID 46897844, see Table 1). Considering the different conducted screening analyses separately, each type of strategy uniquely identified at least one of the confirmed inhibitors: (1) The combination of molecular docking and ligand similarity screening on the ZINC database identified the inhibitor rottlerin among 18 compounds tested, (2) the screening of the MolPort database using fast docking approaches detected another inhibitor (compound M-1805) out of 18 tested candidates, and (3) the screening of the MolPort library using machine learning identified a further inhibitor out of 20 assessed compounds. The complete list of active compounds, including their names, vendor ID, IC$_{50}$ values and 2D structure representations are shown in Table 1. Detailed assay

validation results and dose-response curves for these inhibitors are provided in the Supporting Information.

ADMETox and bioavailability properties of the 3CLpro screening assay hits

While the identified inhibitors did not display a higher activity than the currently available most potent inhibitor GC-376 / GC-373, used as reference compound, multiple of the confirmed actives are natural compounds with favorable bioavailability and ADMETox (Absorption, Distribution, Metabolism, Excretion and Toxicity) properties, that may provide a basis for follow-up structure design optimization efforts or further ligand-based similarity screening in independent compound databases.

To compare all actives in terms of ADME and physicochemical characteristics, corresponding parameters of the confirmed inhibitors were estimated computationally using the software SwissADME (see Table 2 for a summary of key features and Figures S4 to S11 in the Supporting Information for a more comprehensive overview of parameters). This analysis suggested that a subset of compounds, including M-8524, baicalein and luteolin, fulfil multiple typical properties of drug-like, orally bioavailable compounds in terms of the drug-likeness scores proposed by Lipinksi et al. [72], Ghose et al. [73], Veber et al. [74], Egan et al. [75], Muegge et al. [76], and have Abbott Bioavailability Scores above 0.5 [77]. Moreover, some of these compounds also pass all or most PAINS and Brenk's filters [68,69] or display lead-like properties (250 g/mol ≤ molecular weight ≤ 400 g/mol, xlogP ≤ 3.5, num. rotatable bonds ≤ 7) [78], potentially providing a basis for further structural and chemical optimization. By contrast, the reference compound GC-376 is not drug-like

or lead-like according to these scores and has a low bioavailability score (0.17, see Table 2 and Supporting Information).

Table 2: Estimated drug- and lead-likeness and bioavailabilty scores (bioavailability is low = below 0.25, medium = between 0.25 to 0.75, high = above 0.75) of the confirmed 3CLpro inhibitors as estimated using the SwissADME software (more detailed information on the specific score violations and alerts as well as other physicochemical and ADME estimations can be found in the Supporting Information). Passed filters are highlighted in green color, failed tests are marked in red color.

Compounds	GC-376	M-8524	rottlerin	M-1805	amento-flavone	baicalein	luteolin	pectolinarin
Druglikeness (Lipinski)	No (2 violations)	Yes	Yes (1 violation)	Yes	No (2 violations)	Yes	Yes	No (3 violations)
Druglikeness (Ghose)	No (1 violation)	Yes	No (2 violations)	Yes	No (2 violations)	Yes	Yes	No (4 violations)
Druglikeness (Veber)	No (2 violations)	Yes	No (1 violation)	No (1 violation)	No (1 violation)	Yes	Yes	No (1 violation)
Druglikeness (Egan)	No (1 violation)	Yes	No (1 violation)	No (1 violation)	No (1 violation)	Yes	Yes	No (1 violation)
Druglikeness (Muegge)	No (1 violation)	Yes	No (1 violation)	No (1 violation)	No (3 violations)	Yes	Yes	No (4 violations)
Bioavailability Score	low	medium	medium	low	low	medium	medium	low
PAINS	0 alerts	0 alerts	0 alerts	2 alerts	0 alerts	1 alert	1 alert	0 alerts
Brenk	1 alert	0 alerts	1 alert	3 alerts	0 alerts	1 alert	1 alert	0 alerts
Lead-likeness	No (2 violations)	No (3 violations)	No (2 violations)	No (1 violation)	No (2 violations)	Yes	Yes	No (2 violations)

Apart from the computationally estimated ADME properties, prior information on bioavailability and ADMETox characteristics was available for some of the natural products among the confirmed inhibitors. The natural compound with the lowest IC_{50} value, rottlerin, is derived from the powder that covers the capsules of the

tree *Mallotus phillippinensis* (also known as Indian Kamala, Rottlera tree, or monkey-faced tree) [79], which mainly occurs in Asia, Afghanistan and Australia. The powder has traditionally been used as antiparasitic agent against the tapeworm in India for multiple centuries, providing a first indication of favorable safety properties. In mouse model studies, rottlerin was investigated as a preventive or adjuvant supplement for pancreatic cancer [80], as a protective agent against cisplatin-induced nephrotoxicity [81], and as a potential medication in a psoriasis model, where it was well tolerated with no significant changes in bodyweight [82]. Tissue bioavailability and pharmacokinetic analyses *in vitro* and *in vivo* suggest that rottlerin is efficiently absorbed in cells and tissues [80].

The natural product with the second lowest IC50 is amentoflavone, which had previously already been reported to inhibit the 3CLpro protein from SARS-CoV (the virus from the 2002-2004 SARS outbreak) [42]. However, a later study suggested that the binding reaction results from a non-specific aggregate formation or complexation, because no effective inhibition was observed in the presence of 0.01% Triton X-100 [44]. Amentoflavone is a biflavonoid contained in several plant species including *Ginkgo biloba*, *Hypericum perforatum* (St. John's wort), *Xerophyta plicata* and *Chamaecyparis obtusa*. No detailed prior toxicological studies of amentoflavone could be identified, but several bioactivities have been reported in the biomedical literature, including anti-viral effects [83,84].

Among the other natural compounds confirmed to bind to SARS-CoV-2 3CLpro, baicalein displays some of the most favorable drug-likeness scores (see Table 2). This flavonoid is found in the dried roots of the plant *Scutellaria baicalensis (S. baicalensis) Georgi* [85], and was previously already reported to display an antiviral activity against

24

SARS-CoV *in vitro* [86] and to inhibit the SARS-CoV-2 3CL protease *in vitro* [41]. The use of baicalein containing roots was widespread in traditional Chinese herbal medicine over centuries, and a wide range of pharmacological activities have been identified. These include antiviral activities were reported for further virus species apart from SARS corona viruses, including dengue virus [87,88], H5N1 influenza A virus [89], and Japanese encephalitis virus [90].
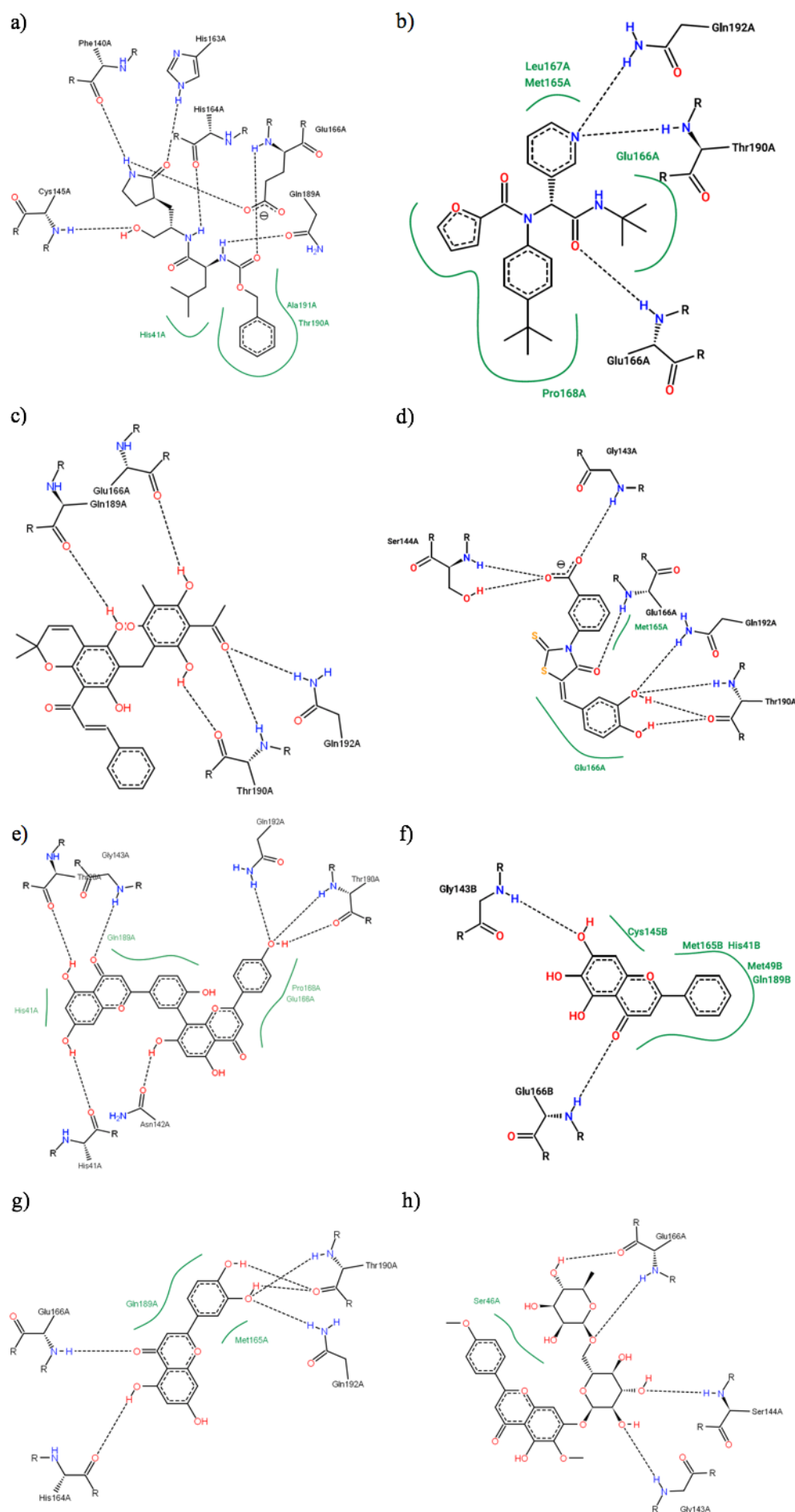
Luteolin, a structurally similar compound to baicalein, also displayed similar estimated ADME properties in terms of favorable drug-likeness and bioavailability scores (see Table 2), and an inhibitory effect of luteolin on SARS-CoV 3CLpro was observed in a previous study using a FRET assay (IC50 = 20.2 μM) [42]. Regarding the bioavailability of luteolin, oral administration of pure luteolin in rats (14.3 mg/kg) has been shown to result in a limited peak plasma concentration of 1.97 ± 0.15 μg/mL, which was increased to 8.34 ± 0.98 μg/mL when delivering the compound in peanut hull extracts [91]. Luteolin is contained in small quantities in both medicinal plants and commonly consumed vegetables and spices (e.g. broccoli, thyme, pepper, and celery), and displays no mutagenic effects in the Ames test in contrast to other flavonoids [92], such as quercetin. Interestingly, quercetin, which only differs structurally from luteolin by the position and number of hydroxyl groups, was also reported to bind to SARS-CoV 3CLpro [42], but with a slightly higher IC50 than luteolin (IC$_{50}$ = 23.8 μM). When testing quercetin as a candidate inhibitor of SARS-CoV-2 3CLpro in the FRET analyses reported here, it did however not show any activity. This suggests that the hydroxyl group positions in flavonoids are an important determinant of their activity for SARS-CoV-2 3CLpro.

Finally, the last natural product confirmed to bind to SARS-CoV-2 3CLpro is pectolinarin. It was previously already found to block the enzymatic activity of SARS-CoV 3CL protease according to a FRET protease assay, using a similar approach as in the study presented here [44]. The compound is isolated from plants of the genus *Cirsium*. Specifically, the plant *Cirsium setidens*, which contains pectolinarin as a major active compound, has been used in traditional Korean medicine against hypertension, hemostasis, hematoma and hematuria [93]. Regarding prior pharmacokinetics studies for pectolinarin, after oral administration of 6 mL/kg *Cirsium japonicum DC* extract in rats, the maximum plasma concentration of the component pectolinarin was 877 ±97 ng/mL, reached after 5 min. [94]. However, pectolinarin displays low drug- and lead-likeness and bioavailability scores in the computational estimations (see Table 2).

Pharmacophore model for 3CLpro small molecule inhibitors

In order to generate a pharmacophore model that describes characteristic features of 3CLpro small molecule inhibitors, we investigated the interactions of the identified inhibitors with residues in the receptor binding pocket using the best scoring docking pose for each compound according to the binding affinity estimation by the software HYDE. For the reference inhibitor GC-376 / GC-373 used for comparison, the relevant pose was derived from a crystal structure which contains this compound in complex with 3CLPro (PDB ID: 7D1M). Similarly, for compound baicalein a crystal structure of the complex with 3CLpro was already available (PDB ID: 6M2N) and used to extract the binding pose. Figure 2 shows the 2D representations of the estimated hydrogen

bond interactions (dotted lines) and hydrophobic contacts (green lines) for each

inhibitor in the 3CLPro binding pocket as determined using the software PoseView
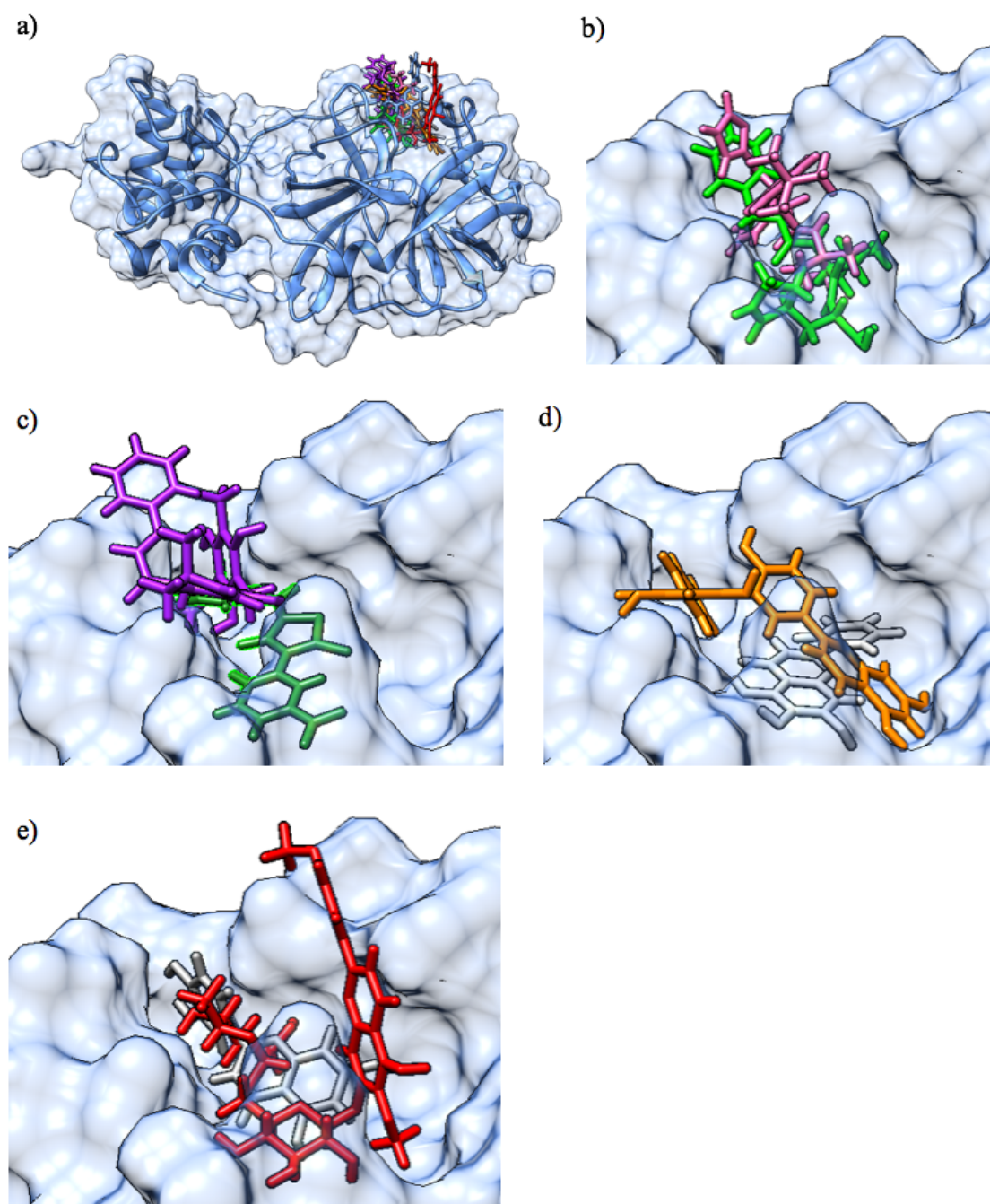
[52].

Figure 2. 2-dimensional representations of the hydrogen bond interactions (dotted lines) and hydrophobic contacts (green lines) between confirmed small molecule inhibitors and residues in the 3CLPro binding pocket: a) GC-373, b) M-8524, c) rottlerin, d) M-1805, e) amentoflavone, f) baicalein, g) luteolin, h) pectolinarin. Plots were generated using the software PoseView. The inhibitor GC-376 / GC-373 is shown in the pose derived from a crystal structure of 3CLPro in complex with this compound (PDB ID: 7D1M). All other sub-figures represent the best scoring docking poses for the corresponding compounds according to the HYDE binding affinity estimation score.

An overview of the binding pocket residues involved in these protein-ligand interactions is provided in Table 3, highlighting all interactions shared by at least two compounds in color, and representing identical residues by identical colors. Most hydrogen bond interactions and hydrophobic contacts with binding pocket residues are shared by multiple ligands, suggesting that they reflect a common binding mode and a characteristic signature of interactions that favor stable ligand binding. The residues most frequently participating in these protein-ligand interactions are Glu166 (involved in hydrogen bonds for 8 inhibitors, and in hydrophobic contacts for 3 inhibitors), Thr190 (H-bonds: 5, Contacts: 1), Gln189 (H-bonds: 2, Contacts: 3) and Gln192 (H-bonds: 5). Interestingly, the two residues His41 and Cys145 which have previously been confirmed to be critical for catalysis [95] are also involved in hydrogen bond interactions with some of the inhibitors (His41 for amentoflavone; Cys145 for GC-376 / GC-373) and hydrophobic contacts (His41 for GC-376 / GC-373, amentoflavone, and baicalein; Cys145 for baicalein), and these compounds may directly interfere with the catalytic mechanism. Overall, both the shared interactions (see Table 3) and the graphic overlay of the docked or crystal structure derived ligand

conformations (see Figure 3) suggest that the confirmed inhibitors use a similar binding mode to engage the 3CLpro binding pocket.

Table 3. Overview of hydrogen bond interactions (2nd column) and hydrophobic contacts (3rd column) between the inhibitors and residues in the 3CLPro binding pocket (inferred by applying the PoseView software with default settings). The residue 3-letter codes and numbers correspond to the 3CLPro amino acids involved in the interaction type indicated in the column header (residues are sorted by increasing position in the 3CLpro amino acid sequence). All residues shown in color are involved in binding interactions for at least two different inhibitors, where identical colors represent identical residues. These shared interactions across multiple ligands may represent critical features that favor the binding of small molecules in the 3CLPro binding pocket.

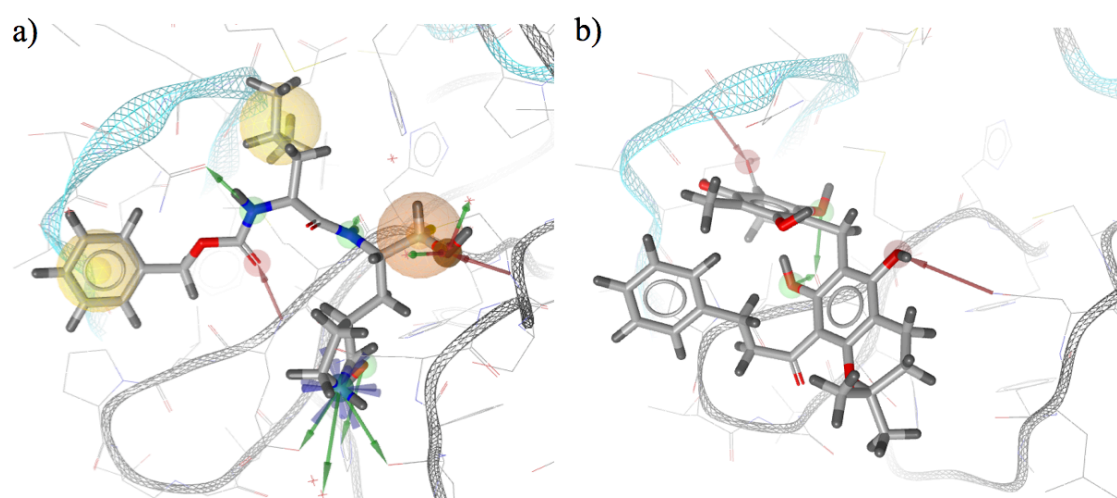| Compounds	H-bonds	Contacts
GC-376 / GC-373	Phe140, Cys145, His163, His164, Glu166, Gln189	His41, Thr190, Ala191
rottlerin	Glu166, Gln189, Thr190, Gln192	-
M-8524	Glu166, Thr190, Gln192	Met165, Glu166, Leu167, Pro168
M-1805	Ser144, Gly143, Glu166, Thr190, Gln192	Met165, Glu166
amentoflavone	His41, Asn142, Gly143, Thr190, Gln192	His41, Glu166, Pro168, Gln189
baicalein	Glu166, Gly143	His41, Met49, Cys145, Met165, Gln189
luteolin	His164, Glu166, Thr190, Gln192	Met165, Gln189
pectolinarin	Gly143, Ser144, Glu166	Ser45

Figure 3. a) Molecular surface representation of the 3CLpro protein with an overlay of all confirmed

actives in the binding pocket (top right) in their best scoring docking conformations (only for GC-376 /

GC-373 and baicalein, crystal structures of the protein-ligand complex were available and used instead

of molecular docking derived conformations). The 3CLpro secondary structure is displayed as a blue

ribbon, surrounded by the solvent excluded molecular surface representation in transparent blue, and

with the colored ligands shown in a stick representation. b) Larger scale representation of the overlaid

pair of ligands with the lowest IC_{50} values: GC-376 (light green) and M-8524 (pink) in the 3CLpro binding

pocket (top right part of figure 3 a); c) overlaid pair of ligands rottlerin (purple) and M-1805 (dark green); d) overlaid pair of ligands amentoflavone (orange) and baicalein (light gray); e) overlaid pair of ligands luteolin (dark gray) and pectolinarin (red).

Next, we created dedicated pharmacophore models for each of the inhibitors using the structure-based pharmacophore design approach in the software LigandScout [96]. Two example pharmacophore models are shown in Figure 4 for the reference compound GC-376 / GC-373 (Figure 4 a), and the newly identified inhibitor rottlerin (Figure 4 b), respectively. These two compounds occupy a similar space in the binding pocket, like most identified inhibitors in their docked binding conformation (see Figure 3), but engage at least partly in different hydrogen bond and hydrophobic interactions with the residues in the pocket. Thus, by merging the pharmacophore models for these and all other confirmed inhibitors into a single model, further virtual screening and structural design optimization efforts may exploit the unified model to identify new inhibitors with suitable steric properties that engage in more energetically favorable combinations of interactions than those covered by the already identified actives. Therefore, the pharmacophore models for the individual ligands were integrated by aligning the structures and their associated pharmacophores by receptor-derived reference points and interpolating the overlapping features, using the default settings in the LigandScout software. In contrast to the models for the individual inhibitors, the resulting merged pharmacophore model does not lend itself to direct interpretation, due to its larger coverage of potential binding interactions that can be exploited by a ligand. However, its more comprehensive coverage of potential interactions provides a computational resource for further screening studies

on independent compound databases that is more informative than individual structures of protein-ligand complexes. The merged pharmacophore model has therefore been made available in the "Compressed Pharmaceutical Markup Language" (PMZ) format on GitHub (https://github.com/eglaab/3clpro). The reader should note that this ligand-based pharmacophore model is specific to the inhibitors identified in the present project, and should therefore ideally be considered in combination with other published pharmacophore models exploiting additional information sources, e.g. a recently proposed receptor-based pharmacophore definition for 3CLpro that combines information from molecular simulations and crystallographic studies [25].

Figure 4. a) Pharmacophore model for 3CLpro derived from the reference inhibitor GC-376 / GC-373 using the software LigandScout (conformation obtained from the PDB crystal structure 7D1M after pre-processing with the software Schrödinger Maestro, see Methods). The yellow spheres represent hydrophobic interactions, the red spheres and arrows correspond to hydrogen bond acceptors, and the green spheres and arrows to hydrogen bond donors. b) Pharmacophore model for 3CLpro derived from the inhibitor rottlerin using the software LigandScout (conformation obtained from the best scoring pose in molecular docking according to the HYDE scoring approach, see Methods). While the comparison of rottlerin and GC-376 / GC-373 suggests that they occupy a similar space in the 3CLpro

binding pocket and share a hydrogen bond interaction with the residue Glu166, most interactions are

distinct. This may open up possibilities for the screening of new compounds that exploit interactions

from the pharmacophore models of both the GC-376 / GC-373 and rottlerin ligand.

CONCLUSIONS

The SARS-CoV-2 3CLpro protein is one of the main drug targets of interest for COVID-19, due to its critical role in viral replication, the availability of multiple high quality protein crystal structures and the prior identification of first small molecule inhibitors as a basis to computationally screen for inhibitors with improved inhibitory activity, bioavailability and ADMETox characteristics.

The combined computational and experimental analyses presented here reveal new natural and synthetic compounds inhibiting 3CLpro with micromolar activity, e.g. rottlerin and M-8524, and provide a pharmacophore model that describes key structural and chemical properties of active compounds. Both this pharmacophore and the confirmed hits provide a resource to support follow-up efforts on the structural design of more potent and selective 3CLpro inhibitors and similarity-based inhibitor screening in additional compound databases. The pharmacophore analyses suggest that many of the 3CLpro inhibitors share hydrogen bond and hydrophobic interactions with binding pocket residues, including interactions with the two residues His41 and Cys145, that have previously been confirmed to be critical for catalysis.

Apart from the new inhibitors identified through the screening of the ZINC, SWEETLEAD and MolPort databases, we also assessed compounds previously proposed as SARS-CoV 3CLPro inhibitors in the literature in terms of their SARS-CoV-2 3CLPro inhibitory activity, confirming amentoflavone, baicalein, luteolin and pectolinarin as actives (albeit with lower affinities then GC-376 / GC-373, rottlerin and M-8524, among others), and rejecting several other candidate compounds as actives (in the lists of tested compounds in the Supporting Information, the confirmed compounds are all marked with a star symbol; the compounds which could not be

35

assessed in the assay due to high background fluorescence are marked in blue, and all other compounds were invalidated). Analyses of ADMETox and physicochemical parameters of the confirmed hit compounds show that these compounds differ significantly with regard to relevant known or computationally estimated properties, and that a subset of the hits displays favorable bioavailability and safety characteristics in terms of the prior knowledge available.

Regarding the computational methodological aspects of the project, as part of the virtual screening we have tested different screening approaches, including the integration of molecular docking and ligand similarity screening, the combined application of fast docking approaches without prior compound library filtering, and the use of machine learning for screening. The observation that each of these approaches uniquely identified at least one of the experimentally confirmed inhibitors suggests that the different screening strategies provide independent and complementary information, which can help to increase the overall number and diversity of the identified active compounds. Identifying structurally and chemically diverse active compounds with a similar binding mode is important for the creation of more comprehensive integrated pharmacophore models.

Limitations of the computational and experimental screening approach employed include a restricted scalability of the *in vitro* assay for assessing 3CLpro inhibitory activity, which has recently been addressed by the development of an optimized assay for high-throughput screening of 3CLpro [20], and limitations in terms of the size of the compound library and the conformational search space that could be explored using high-performance computing facilities available in a typical academic setting, which may be addressed using recent dedicated supercomputer-based screening

approaches [24–26]. Extending 3CLpro virtual screening to supercomputer-based methodologies has also recently been shown to enable an improved modeling of receptor flexibility using ensemble docking [24], extensive MD simulations to generate high-resolution conformational ensembles [25], and the application of more advanced polarizable force fields [26].

As a next step, extended/further screening and structural optimization analyses for 3CLpro inhibitors will be required. This will help to pave the way for additional activity assessments in preclinical models and the subsequent development of lead compounds.

DATA AND SOFTWARE AVAILABILITY

The Supporting Information contains the lists of all experimentally assessed candidate 3CLPro inhibitors, the dose-response curves and structures in SMILES format for all experimentally confirmed active compounds, the results for the validation analyses of the FRET-based 3CLPro *in vitro* assay and the reference inhibitor GC-376, and the detailed results for the physicochemical and ADME analyses. Scripts including the commands and parameters for the molecular docking analyses, the ligand similarity search, the machine learning based screening, the configuration settings used for the software NAMD, as well as a list of all used software tools and their versions, and exemplary video animations of MD simulations for confirmed inhibitors are available on GitHub (https://github.com/eglaab/3clpro).

SUPPORTING INFORMATION

- Tables S1-S5: Lists of experimentally assessed candidate 3CLPro small molecule inhibitors

- Figures S1-S2: Validation of the FRET assay and the reference compound

- Figure S3: Dose-response curves for the active compounds

- Figures S4-S11: Physicochemical and ADME analyses for the active compounds

- Used software tools and versions for the virtual screening analyses

- Step-by-step description of the virtual screening analyses

References

1. Matthay MA, Thompson BT. Dexamethasone In Hospitalised Patients With COVID-19: Addressing Uncertainties. Lancet Respir. Med. 2020; 8:1170–1172

2. Beigel JH, Tomashek KM, Dodd LE, Mehta AK, Zingman BS, Kalil AC, Hohmann E, Chu HY, Luetkemeyer A, Kline S, Lopez de Castilla D, Finberg RW, Dierberg K, Tapson V, Hsieh L, Patterson TF, Paredes R, Sweeney DA, Short WR, Touloumi G, Lye DC, Ohmagari N, Oh M, Ruiz-Palacios GM, Benfield T, Fätkenheuer G, Kortepeter MG, Atmar RL, Creech CB, Lundgren J, Babiker AG, Pett S, Neaton JD, Burgess TH, Bonnett T, Green M, Makowski M, Osinusi A, Nayak S, Lane HC. Remdesivir For The Treatment Of Covid-19 — Final Report. N. Engl. J. Med. 2020; 383:1813–1826

3. Spinner CD, Gottlieb RL, Criner GJ, Arribas López JR, Cattelan AM, Soriano Viladomiu A, Ogbuagu O, Malhotra P, Mullane KM, Castagna A, Chai LYA, Roestenberg M, Tsang OTY, Bernasconi E, Le Turnier P, Chang SC, Sengupta D, Hyland RH, Osinusi AO, Cao H, Blair C, Wang H, Gaggar A, Brainard DM, McPhail MJ, Bhagani S, Ahn MY, Sanyal AJ, Huhn G, Marty FM. Effect Of Remdesivir Vs Standard Care On Clinical Status At 11 Days In Patients With Moderate COVID-19: A Randomized Clinical Trial. JAMA - J. Am. Med. Assoc. 2020; 324:1048–1057

4. . Repurposed Antiviral Drugs For Covid-19 — Interim WHO Solidarity Trial Results. N. Engl. J. Med. 2021; 384:497–511

5. McCreary EK, Meyer NJ. Covid-19 Controversies: The Tocilizumab Chapter. BMJ 2021; 372:n244

6. Schlesinger N, Firestein BL, Brunetti L. Colchicine In COVID-19: An Old Drug, New Use. Curr. Pharmacol. Reports 2020; 6:137–145

7. Weinreich DM, Sivapalasingam S, Norton T, Ali S, Gao H, Bhore R, Musser BJ, Soo Y, Rofail D, Im J, Perry C, Pan C, Hosain R, Mahmood A, Davis JD, Turner KC, Hooper AT, Hamilton JD, Baum A, Kyratsous CA, Kim Y, Cook A, Kampman W, Kohli A, Sachdeva Y, Graber X, Kowal B, DiCioccio T, Stahl N, Lipsich L, Braunstein N, Herman G, Yancopoulos GD. REGN-COV2, A Neutralizing Antibody Cocktail, In Outpatients With Covid-19. N. Engl. J. Med. 2021; 384:238–251

8. Roback JD, Guarner J. Convalescent Plasma To Treat COVID-19: Possibilities And Challenges. JAMA - J. Am. Med. Assoc. 2020; 323:1561–1562

9. Hoffmann M, Kleine-Weber H, Schroeder S, Krüger N, Herrler T, Erichsen S, Schiergens TS, Herrler G, Wu NH, Nitsche A, Müller MA, Drosten C, Pöhlmann S. SARS-CoV-2 Cell Entry Depends On ACE2 And TMPRSS2 And Is Blocked By A Clinically Proven Protease Inhibitor. Cell 2020; 181:271-280.e8

10. Wu C, Zheng M, Yang Y, Gu X, Yang K, Li M, Liu Y, Zhang Q, Zhang P, Wang Y, Wang Q, Xu Y, Zhou Y, Zhang Y, Chen L, Li H. Furin: A Potential Therapeutic Target For COVID-19. iScience 2020; 23:101642

11. Mody V, Ho J, Wills S, Mawri A, Lawson L, Ebert MCCJC, Fortin GM, Rayalam S, Taval S. Identification Of 3-Chymotrypsin Like Protease (3CLPro) Inhibitors As Potential Anti-SARS-CoV-2 Agents. Commun. Biol. 2021; 4:93

12. Gao X, Qin B, Chen P, Zhu K, Hou P, Wojdyla JA, Wang M, Cui S. Crystal Structure Of

SARS-CoV-2 Papain-Like Protease. Acta Pharm. Sin. B 2021; 11:237–245

13. Yin W, Mao C, Luan X, Shen DD, Shen Q, Su H, Wang X, Zhou F, Zhao W, Gao M, Chang S, Xie YC, Tian G, Jiang HW, Tao SC, Shen J, Jiang Y, Jiang H, Xu Y, Zhang S, Zhang Y, Xu HE. Structural Basis For Inhibition Of The RNA-Dependent RNA Polymerase From SARS-CoV-2 By Remdesivir. Science 2020; 368:1499–1504

14. White MA, Lin W, Cheng X. Discovery Of COVID-19 Inhibitors Targeting The SARS-CoV-2 Nsp13 Helicase. J. Phys. Chem. Lett. 2020; 9144–9151

15. Huang Y, Yang C, Xu X feng, Xu W, Liu S wen. Structural And Functional Properties Of SARS-CoV-2 Spike Protein: Potential Antivirus Drug Development For COVID-19. Acta Pharmacol. Sin. 2020; 41:1141–1149

16. Issa E, Merhi G, Panossian B, Salloum T, Tokajian S. SARS-CoV-2 And ORF3a: Nonsynonymous Mutations, Functional Domains, And Viral Pathogenesis. mSystems 2020; 5:e00266-20

17. Schwarz S, Wang K, Yu W, Sun B, Schwarz W. Emodin Inhibits Current Through SARS-Associated Coronavirus 3a Protein. Antiviral Res. 2011; 90:64–69

18. Ma C, Sacco MD, Hurst B, Townsend JA, Hu Y, Szeto T, Zhang X, Tarbet B, Marty MT, Chen Y, Wang J. Boceprevir, GC-376, And Calpain Inhibitors II, XII Inhibit SARS-CoV-2 Viral Replication By Targeting The Viral Main Protease. Cell Res. 2020; 30:678–692

19. Mukherjee P, Shah F, Desai P, Avery M. Inhibitors Of SARS-3CLpro: Virtual Screening, Biological Evaluation, And Molecular Dynamics Simulation Studies. J. Chem. Inf. Model. 2011; 51:1376–1392

20. Breidenbach J, Lemke C, Pillaiyar T, Schäkel L, Al Hamwi G, Diett M, Gedschold R, Geiger N, Lopez V, Mirza S, Namasivayam V, Schiedel AC, Sylvester K, Thimm D, Vielmuth C, Phuong Vu L, Zyulina M, Bodem J, Gütschow M, Müller CE. Targeting The Main Protease Of SARS-CoV-2: From The Establishment Of High Throughput Screening To The Design Of Tailored Inhibitors. Angew. Chemie - Int. Ed. 2021; 60:10423–10429

21. Zhang CH, Stone EA, Deshmukh M, Ippolito JA, Ghahremanpour MM, Tirado-Rives J, Spasov KA, Zhang S, Takeo Y, Kudalkar SN, Liang Z, Isaacs F, Lindenbach B, Miller SJ, Anderson KS, Jorgensen WL. Potent Noncovalent Inhibitors Of The Main Protease Of SARS-CoV-2 From Molecular Sculpting Of The Drug Perampanel Guided By Free Energy Perturbation Calculations. ACS Cent. Sci. 2021; 7:467–475

22. Irwin JJ, Shoichet BK. ZINC - A Free Database Of Commercially Available Compounds For Virtual Screening. J. Chem. Inf. Model. 2005; 45:177–182

23. Novick PA, Ortiz OF, Poelman J, Abdulhay AY, Pande VS. SWEETLEAD: An In Silico Database Of Approved Drugs, Regulated Chemicals, And Herbal Isolates For Computer-Aided Drug Discovery. PLoS One 2013; 8:e79568

24. Acharya A, Agarwal R, Baker MB, Baudry J, Bhowmik D, Boehm S, Byler KG, Chen SY, Coates L, Cooper CJ, Demerdash O, Daidone I, Eblen JD, Ellingson S, Forli S, Glaser J, Gumbart JC, Gunnels J, Hernandez O, Irle S, Kneller DW, Kovalevsky A, Larkin J, Lawrence TJ, Legrand S, Liu SH, Mitchell JC, Park G, Parks JM, Pavlova A, Petridis L, Poole D, Pouchard L, Ramanathan A, Rogers DM, Santos-Martins D, Scheinberg A, Sedova A, Shen Y, Smith JC, Smith MD, Soto C, Tsaris A, Thavappiragasam M, Tillack AF, Vermaas J V., Vuong VQ, Yin J, Yoo S, Zahran M, Zanetti-Polzi L. Supercomputer-Based Ensemble Docking Drug Discovery

Pipeline With Application To Covid-19. J. Chem. Inf. Model. 2020;

25. Gossen J, Albani S, Hanke A, Joseph BP, Bergh C, Kuzikov M, Costanzi E, Manelfi C, Storici P, Gribbon P, Beccari AR, Talarico C, Spyrakis F, Lindahl E, Zaliani A, Carloni P, Wade RC, Musiani F, Kokh DB, Rossetti G. A Blueprint For High Affinity SARS-CoV-2 Mpro Inhibitors From Activity-Based Compound Library Screening Guided By Analysis Of Protein Dynamics. ACS Pharmacol. Transl. Sci. 2021;

26. Jaffrelot Inizan T, Célerse F, Adjoua O, El Ahdab D, Jolly LH, Liu C, Ren P, Montes M, Lagarde N, Lagardère L, Monmarché P, Piquemal JP. High-Resolution Mining Of The SARS-CoV-2 Main Protease Conformational Space: Supercomputer-Driven Unsupervised Adaptive Sampling. Chem. Sci. 2021;

27. Pelly S, Liotta D. Potent SARS-CoV-2 Direct-Acting Antivirals Provide An Important Complement To COVID-19 Vaccines. ACS Cent. Sci. 2021;

28. Berman HM, Battistuz T, Bhat TN, Bluhm WF, Bourne PE, Burkhardt K, Feng Z, Gilliland GL, Iype L, Jain S, Fagan P, Marvin J, Padilla D, Ravichandran V, Schneider B, Thanki N, Weissig H, Westbrook JD, Zardecki C. The Protein Data Bank. Acta Crystallogr. Sect. D Biol. Crystallogr. 2002; 58:899–907

29. El-Baba TJ, Lutomski CA, Kantsadi AL, Malla TR, John T, Mikhailov V, Bolla JR, Schofield CJ, Zitzmann N, Vakonakis I, Robinson C V. Allosteric Inhibition Of The SARS-CoV-2 Main Protease: Insights From Mass Spectrometry Based Assays. Angew. Chemie - Int. Ed. 2020; 59:23544–23548

30. Günther S, Reinke PYA, Fernández-García Y, Lieske J, Lane TJ, Ginn HM, Koua FHM, Ehrt C, Ewert W, Oberthuer D, Yefanov O, Meier S, Lorenzen K, Krichel B, Kopicki J-D, Gelisio L, Brehm W, Dunkel I, Seychell B, Gieseler H, Norton-Baker B, Escudero-Pérez B, Domaracky M, Saouane S, Tolstikova A, White TA, Hänle A, Groessler M, Fleckenstein H, Trost F, Galchenkova M, Gevorkov Y, Li C, Awel S, Peck A, Barthelmess M, Schlünzen F, Lourdu Xavier P, Werner N, Andaleeb H, Ullah N, Falke S, Srinivasan V, França BA, Schwinzer M, Brognaro H, Rogers C, Melo D, Zaitseva-Doyle JJ, Knoska J, Peña-Murillo GE, Mashhour AR, Hennicke V, Fischer P, Hakanpää J, Meyer J, Gribbon P, Ellinger B, Kuzikov M, Wolf M, Beccari AR, Bourenkov G, von Stetten D, Pompidor G, Bento I, Panneerselvam S, Karpics I, Schneider TR, Garcia-Alai MM, Niebling S, Günther C, Schmidt C, Schubert R, Han H, Boger J, Monteiro DCF, Zhang L, Sun X, Pletzer-Zelgert J, Wollenhaupt J, Feiler CG, Weiss MS, Schulz E-C, Mehrabi P, Karničar K, Usenik A, Loboda J, Tidow H, Chari A, Hilgenfeld R, Uetrecht C, Cox R, Zaliani A, Beck T, Rarey M, Günther S, Turk D, Hinrichs W, Chapman HN, Pearson AR, Betzel C, Meents A. X-Ray Screening Identifies Active Site And Allosteric Inhibitors Of SARS-CoV-2 Main Protease. Science (80-.). 2021; 372:642–646

31. Verma S, Pandey AK. Factual Insights Of The Allosteric Inhibition Mechanism Of SARS-CoV-2 Main Protease By Quercetin: An In Silico Analysis. 3 Biotech 2021; 11:67

32. Wei P, Fan K, Chen H, Ma L, Huang C, Tan L, Xi D, Li C, Liu Y, Cao A, Lai L. The N-Terminal Octapeptide Acts As A Dimerization Inhibitor Of SARS Coronavirus 3C-Like Proteinase. Biochem. Biophys. Res. Commun. 2006; 339:865–872

33. Ding L, Zhang XX, Wei P, Fan K, Lai L. The Interaction Between Severe Acute Respiratory Syndrome Coronavirus 3C-Like Proteinase And A Dimeric Inhibitor By Capillary Electrophoresis. Anal. Biochem. 2005; 343:159–165

34. Eisenberg D, Lüthy R, Bowie JU. VERIFY3D: Assessment Of Protein Models With Three-

Dimensional Profiles. Methods Enzymol. 1997; 277:396–406

35. Hooft RWW, Vriend G, Sander C, Abola EE. Errors In Protein Structures. Nature 1996; 381:272

36. Laskowski RA, MacArthur MW, Thornton JM. PROCHECK : Validation Of Protein-Structure Coordinates. Crystallogr. Biol. Macromol. 2012; 684–687

37. Glaab E. Building A Virtual Ligand Screening Pipeline Using Free Software: A Survey. Brief. Bioinform. 2016; 17:352–366

38. Santos-Martins D, Solis-Vasquez L, Tillack AF, Sanner MF, Koch A, Forli S. Accelerating AutoDock 4 With GPUs And Gradient-Based Local Search. J. Chem. Theory Comput. 2021; 17:1060–1073

39. Menéndez CA, Byléhn F, Perez-Lemus GR, Alvarado W, de Pablo JJ. Molecular Characterization Of Ebselen Binding Activity To SARS-CoV-2 Main Protease. Sci. Adv. 2020; 6:eabd0345

40. Jin Z, Du X, Xu Y, Deng Y, Liu M, Zhao Y, Zhang B, Li X, Zhang L, Peng C, Duan Y, Yu J, Wang L, Yang K, Liu F, Jiang R, Yang X, You T, Liu X, Yang X, Bai F, Liu H, Liu X, Guddat LW, Xu W, Xiao G, Qin C, Shi Z, Jiang H, Rao Z, Yang H. Structure Of Mpro From SARS-CoV-2 And Discovery Of Its Inhibitors. Nature 2020; 582:289–293

41. Su H xia, Yao S, Zhao W feng, Li M jun, Liu J, Shang W juan, Xie H, Ke C qiang, Hu H chen, Gao M na, Yu K qian, Liu H, Shen J shan, Tang W, Zhang L ke, Xiao G fu, Ni L, Wang D wen, Zuo J ping, Jiang H liang, Bai F, Wu Y, Ye Y, Xu Y chun. Anti-SARS-CoV-2 Activities In Vitro Of Shuanghuanglian Preparations And Bioactive Ingredients. Acta Pharmacol. Sin. 2020; 41:1167–1177

42. Ryu YB, Jeong HJ, Kim JH, Kim YM, Park JY, Kim D, Naguyen TTH, Park SJ, Chang JS, Park KH, Rho MC, Lee WS. Biflavonoids From Torreya Nucifera Displaying SARS-CoV 3CLpro Inhibition. Bioorganic Med. Chem. 2010; 18:7940–7947

43. Lin CW, Tsai FJ, Tsai CH, Lai CC, Wan L, Ho TY, Hsieh CC, Chao PDL. Anti-SARS Coronavirus 3C-Like Protease Effects Of Isatis Indigotica Root And Plant-Derived Phenolic Compounds. Antiviral Res. 2005; 68:36–42

44. Jo S, Kim S, Shin DH, Kim MS. Inhibition Of SARS-CoV 3CL Protease By Flavonoids. J. Enzyme Inhib. Med. Chem. 2020; 35:145–151

45. Park JY, Kim JH, Kwon JM, Kwon HJ, Jeong HJ, Kim YM, Kim D, Lee WS, Ryu YB. Dieckol, A SARS-CoV 3CLpro Inhibitor, Isolated From The Edible Brown Algae Ecklonia Cava. Bioorganic Med. Chem. 2013; 21:3730–3737

46. Kelley BP, Brown SP, Warren GL, Muchmore SW. POSIT: Flexible Shape-Guided Docking For Pose Prediction. J. Chem. Inf. Model. 2015; 55:1771–1780

47. McGann M. FRED Pose Prediction And Virtual Screening Accuracy. J. Chem. Inf. Model. 2011; 51:578–596

48. McGann M. FRED And HYBRID Docking Performance On Standardized Datasets. J. Comput. Aided. Mol. Des. 2012; 26:897–906

49. Kramer B, Rarey M, Lengauer T. Evaluation Of The FlexX Incremental Construction

Algorithm For Protein- Ligand Docking. Proteins Struct. Funct. Genet. 1999; 37:228–241

50. Schneider N, Lange G, Hindle S, Klein R, Rarey M. A Consistent Description Of HYdrogen Bond And DEhydration Energies In Protein-Ligand Complexes: Methods Behind The HYDE Scoring Function. J. Comput. Aided. Mol. Des. 2013; 27:15–29

51. Pettersen EF, Goddard TD, Huang CC, Couch GS, Greenblatt DM, Meng EC, Ferrin TE. UCSF Chimera--A Visualization System For Exploratory Research And Analysis. J. Comput. Chem. 2004; 25:1605–1612

52. Stierand K, Rarey M. PoseView -- Molecular Interaction Patterns At A Glance. J. Cheminform. 2010; 2:P50

53. Nelson MT, Humphrey W, Gursoy A, Dalke A, Kale L V., Skeel RD, Schulten K. NAMD: A Parallel, Object-Oriented Molecular Dynamics Program. Int. J. High Perform. Comput. Appl. 1996; 10:251–268

54. MacKerell AD, Bashford D, Bellott M, Dunbrack RL, Evanseck JD, Field MJ, Fischer S, Gao J, Guo H, Ha S, Joseph-McCarthy D, Kuchnir L, Kuczera K, Lau FTK, Mattos C, Michnick S, Ngo T, Nguyen DT, Prodhom B, Reiher WE, Roux B, Schlenkrich M, Smith JC, Stote R, Straub J, Watanabe M, Wiórkiewicz-Kuczera J, Yin D, Karplus M. All-Atom Empirical Potential For Molecular Modeling And Dynamics Studies Of Proteins. J. Phys. Chem. B 1998; 102:3586–3616

55. Huang J, Mackerell AD. CHARMM36 All-Atom Additive Protein Force Field: Validation Based On Comparison To NMR Data. J. Comput. Chem. 2013; 34:2135–2145

56. Vanommeslaeghe K, Hatcher E, Acharya C, Kundu S, Zhong S, Shim J, Darian E, Guvench O, Lopes P, Vorobyov I, Mackerell AD. CHARMM General Force Field: A Force Field For Drug-Like Molecules Compatible With The CHARMM All-Atom Additive Biological Force Fields. J. Comput. Chem. 2010; 31:671–690

57. Guha R. Chemical Informatics Functionality In R. J. Stat. Softw. 2007; 18:1–16

58. Weininger D. SMILES, A Chemical Language And Information System. 1. Introduction To Methodology And Encoding Rules. J. Chem. Inf. Comput. Sci. 1988; 28:31–36

59. Ivanov J, Polshakov D, Kato-Weinstein J, Zhou Q, Li Y, Granet R, Garner L, Deng Y, Liu C, Albaiu D, Wilson J, Aultman C. Quantitative Structure–activity Relationship Machine Learning Models And Their Applications For Identifying Viral 3Clpro- And RDRP-Targeting Compounds As Potential Therapeutics For Covid-19 And Related Viral Infections. ACS Omega 2020; 5:27344–27358

60. Liaw A, Wiener M. Classification And Regression By RandomForest. R News 2002; 2:18–22

61. Najumudeen AK, Köhnke M, Šolman M, Alexandrov K, Abankwa D. Cellular FRET-Biosensors To Detect Membrane Targeting Inhibitors Of N-Myristoylated Proteins. PLoS One 2013; 8:e66425

62. Gulin-Sarfraz T, Sarfraz J, Karaman DŞ, Zhang J, Oetken-Lindholm C, Duchanoy A, Rosenholm JM, Abankwa D. FRET-Reporter Nanoparticles To Monitor Redox-Induced Intracellular Delivery Of Active Compounds. RSC Adv. 2014; 4:16429–16437

63. Zhang L, Lin D, Kusov Y, Nian Y, Ma Q, Wang J, Von Brunn A, Leyssen P, Lanko K, Neyts J,

De Wilde A, Snijder EJ, Liu H, Hilgenfeld R. α-Ketoamides As Broad-Spectrum Inhibitors Of Coronavirus And Enterovirus Replication: Structure-Based Design, Synthesis, And Activity Assessment. J. Med. Chem. 2020; 63:4562–4578

64. Manoharan G babu, Kopra K, Eskonen V, Härmä H, Abankwa D. High-Throughput Amenable Fluorescence-Assays To Screen For Calmodulin-Inhibitors. Anal. Biochem. 2019; 572:25–32

65. Manoharan GB, Enkvist E, Uri A. Combining Chemical And Genetic Approaches For Development Of Responsive FRET-Based Sensor Systems For Protein Kinases. Biophys. Chem. 2016; 211:39–48

66. Ryu YB, Park SJ, Kim YM, Lee JY, Seo WD, Chang JS, Park KH, Rho MC, Lee WS. SARS-CoV 3CLpro Inhibitory Effects Of Quinone-Methide Triterpenes From Tripterygium Regelii. Bioorganic Med. Chem. Lett. 2010; 20:1873–1876

67. Hsu JTA, Kuo CJ, Hsieh HP, Wang YC, Huang KK, Lin CPC, Huang PF, Chen X, Liang PH. Evaluation Of Metal-Conjugated Compounds As Inhibitors Of 3CL Protease Of SARS-CoV. FEBS Lett. 2004; 574:116–120

68. Baell JB, Holloway GA. New Substructure Filters For Removal Of Pan Assay Interference Compounds (PAINS) From Screening Libraries And For Their Exclusion In Bioassays. J. Med. Chem. 2010; 53:2719–2740

69. Brenk R, Schipani A, James D, Krasowski A, Gilbert IH, Frearson J, Wyatt PG. Lessons Learnt From Assembling Screening Libraries For Drug Discovery For Neglected Diseases. ChemMedChem 2008; 3:435–444

70. Vuong W, Khan MB, Fischer C, Arutyunova E, Lamer T, Shields J, Saffran HA, McKay RT, van Belkum MJ, Joyce MA, Young HS, Tyrrell DL, Vederas JC, Lemieux MJ. Feline Coronavirus Drug Inhibits The Main Protease Of SARS-CoV-2 And Blocks Virus Replication. Nat. Commun. 2020; 11:4282

71. Zhang JH, Chung TDY, Oldenburg KR. A Simple Statistical Parameter For Use In Evaluation And Validation Of High Throughput Screening Assays. J. Biomol. Screen. 1999; 4:67–73

72. Lipinski CA. Lead- And Drug-Like Compounds: The Rule-Of-Five Revolution. Drug Discov. Today Technol. 2004; 1:337–341

73. Ghose AK, Viswanadhan VN, Wendoloski JJ. A Knowledge-Based Approach In Designing Combinatorial Or Medicinal Chemistry Libraries For Drug Discovery. 1. A Qualitative And Quantitative Characterization Of Known Drug Databases. J. Comb. Chem. 1999; 1:55–68

74. Veber DF, Johnson SR, Cheng HY, Smith BR, Ward KW, Kopple KD. Molecular Properties That Influence The Oral Bioavailability Of Drug Candidates. J. Med. Chem. 2002; 45:2615–2623

75. Egan WJ, Merz KM, Baldwin JJ. Prediction Of Drug Absorption Using Multivariate Statistics. J. Med. Chem. 2000; 43:3867–3877

76. Muegge I, Heald SL, Brittelli D. Simple Selection Criteria For Drug-Like Chemical Matter. J. Med. Chem. 2001; 44:1841–1846

77. Martin YC. A Bioavailability Score. J. Med. Chem. 2005; 48:3164–3170

78. Teague SJ, Davis AM, Leeson PD, Oprea T. The Design Of Leadlike Combinatorial Libraries. Angew. Chemie - Int. Ed. 1999; 38:3743–3748

79. Goldklang MP, Perez-Zoghbi JF, Trischler J, Nkyimbeng T, Zakharov SI, Shiomi T, Zelonina T, Marks AR, D'Armiento JM, Marx SO. Treatment Of Experimental Asthma Using A Single Small Molecule With Anti-Inflammatory And BK Channelactivating Properties. FASEB J. 2013; 27:4975–4986

80. Yi Lu Q. Determination Of Rottlerin, A Natural Protein Kinases C Inhibitor, In Pancreatic Cancer Cells And Mouse Xenografts By RP-HPLC Method. J. Chromatogr. Sep. Tech. 2012; 4:100062

81. Pabla N, Dong G, Jiang M, Huang S, Kumar MV, Messing RO, Dong Z. Inhibition Of PKCδ Reduces Cisplatin-Induced Nephrotoxicity Without Blocking Chemotherapeutic Efficacy In Mouse Models Of Cancer. J. Clin. Invest. 2011; 121:2709–2722

82. Min M, Yan BX, Wang P, Landeck L, Chen JQ, Li W, Cai SQ, Zheng M, Man XY. Rottlerin As A Therapeutic Approach In Psoriasis: Evidence From In Vitro And In Vivo Studies. PLoS One 2017; 12:e0190051

83. Li F, Song X, Su G, Wang Y, Wang Z, Jia J, Qing S, Huang L, Wang Y, Zheng K, Wang Y. Amentoflavone Inhibits HSV-1 And ACV-Resistant Strain Infection By Suppressing Viral Early Infection. Viruses 2019; 11:466

84. Ma SC, But PPH, Ooi VEC, He YH, Lee SHS, Lee SF, Lin RC. Antiviral Amentoflavone From Selaginella Sinensis. Biol. Pharm. Bull. 2001; 24:311–312

85. Huang Y, Tsang SY, Yao X, Chen ZY. Biological Properties Of Baicalein In Cardiovascular System. Curr. Drug Targets - Cardiovasc. Haematol. Disord. 2005; 5:177–184

86. Chen F, Chan KH, Jiang Y, Kao RYT, Lu HT, Fan KW, Cheng VCC, Tsui WHW, Hung IFN, Lee TSW, Guan Y, Peiris JSM, Yuen KY. In Vitro Susceptibility Of 10 Clinical Isolates Of SARS Coronavirus To Selected Antiviral Compounds. J. Clin. Virol. 2004; 31:69–75

87. Zandi K, Teoh BT, Sam SS, Wong PF, Mustafa MR, AbuBakar S. Novel Antiviral Activity Of Baicalein Against Dengue Virus. BMC Complement. Altern. Med. 2012; 12:214

88. Moghaddam E, Teoh BT, Sam SS, Lani R, Hassandarvish P, Chik Z, Yueh A, Abubakar S, Zandi K. Baicalin, A Metabolite Of Baicalein With Antiviral Activity Against Dengue Virus. Sci. Rep. 2014; 4:5452

89. Sithisarn P, Michaelis M, Schubert-Zsilavecz M, Cinatl J. Differential Antiviral And Anti-Inflammatory Mechanisms Of The Flavonoids Biochanin A And Baicalein In H5N1 Influenza A Virus-Infected Cells. Antiviral Res. 2013; 97:41–48

90. Johari J, Kianmehr A, Mustafa MR, Abubakar S, Zandi K. Antiviral Activity Of Baicalein And Quercetin Against The Japanese Encephalitis Virus. Int. J. Mol. Sci. 2012; 13:16020–16045

91. Zhou P, Li LP, Luo SQ, Jiang H Di, Zeng S. Intestinal Absorption Of Luteolin From Peanut Hull Extract Is More Efficient Than That From Individual Pure Luteolin. J. Agric. Food Chem. 2008; 56:296–300

92. Czeczot H, Tudek B, Kusztelak J, Szymczyk T, Dobrowolska B, Glinkowska G, Malinowski J, Strzelecka H. Isolation And Studies Of The Mutagenic Activity In The Ames Test Of Flavonoids Naturally Occurring In Medical Herbs. Mutat. Res. Toxicol. 1990; 240:209–216

93. Lee S, Lee DH, Kim JC, Um BH, Sung SH, Jeong LS, Kim YK, Kim SN. Pectolinarigenin, An Aglycone Of Pectolinarin, Has More Potent Inhibitory Activities On Melanogenesis Than Pectolinarin. Biochem. Biophys. Res. Commun. 2017; 493:765–772

94. Zhang Z, Jia P, Zhang X, Zhang Q, Yang H, Shi H, Zhang L. LC-MS/MS Determination And Pharmacokinetic Study Of Seven Flavonoids In Rat Plasma After Oral Administration Of Cirsium Japonicum DC. Extract. J. Ethnopharmacol. 2014; 158:66–75

95. Huang C, Wei P, Fan K, Liu Y, Lai L. 3C-Like Proteinase From SARS Coronavirus Catalyzes Substrate Hydrolysis By A General Base Mechanism. Biochemistry 2004; 43:4568–4574

96. Wolber G, Langer T. LigandScout: 3-D Pharmacophores Derived From Protein-Bound Ligands And Their Use As Virtual Screening Filters. J. Chem. Inf. Model. 2005; 45:160–169